forests

MDPI

Article

Drought Influence on Forest Plantations in Zululand, South Africa, Using MODIS Time Series and Climate Data

Sifiso Xulu [1,2,*], Kabir Peerbhay [1], Michael Gebreslasie [1] and Riyad Ismail [1]

[1] School of Agricultural, Earth and Environmental Sciences, University of KwaZulu-Natal, Westville Campus, Durban 4000, South Africa; Kabir.Peerbhay@sappi.com (K.P.); gebreslasie@ukzn.ac.za (M.G.); Riyad.Ismail@sappi.com (R.I.)

[2] Department of Geography and Environmental Studies, University of Zululand, KwaDlangezwa 3886, South Africa

* Correspondence: xulusi@unizulu.ac.za; Tel.: +27-035-902-6331

Received: 23 June 2018; Accepted: 29 August 2018; Published: 30 August 2018

Abstract: South Africa has a long history of recurrent droughts that have adversely affected its economic performance. The recent 2015 drought has been declared the most serious in 26 years and impaired key agricultural sectors including the forestry sector. Research on the forests' responses to drought is therefore essential for management planning and monitoring. The effects of the latest drought on the forests in South Africa have not been studied and are uncertain. The study reported here addresses this gap by using Moderate Resolution Imaging Spectroradiometer (MODIS)-derived normalized difference vegetation index (NDVI) and precipitation data retrieved and processed using the JavaScript code editor in the Google Earth Engine (GEE) and the corresponding normalized difference infrared index (NDII), Palmer drought severity index (PDSI), and El Niño time series data for KwaMbonambi, northern Zululand, between 2002 and 2016. The NDVI and NDII time series were decomposed using the Breaks for Additive Seasonal and Trend (BFAST) method to establish the trend and seasonal variation. Multiple linear regression and Mann–Kendall tests were applied to determine the association of the NDVI and NDII with the climate variables. Plantation trees displayed high NDVI values (0.74–0.78) from 2002 to 2013; then, they decreased sharply to 0.64 in 2015. The Mann–Kendall trend test confirmed a negative significant (p = 0.000353) trend between 2014 and 2015. This pattern was associated with a precipitation deficit and low NDII values during a strong El Niño phase. The PDSI (−2.6) values indicated severe drought conditions. The greening decreased in 2015, with some forest remnants showing resistance, implying that the tree species had varying sensitivity to drought. We found that the plantation trees suffered drought stress during 2015, although it seems that the trees began to recover, as the NDVI signals rose in 2016. Overall, these results demonstrated the effective use of the NDVI- and NDII-derived MODIS data coupled with climatic variables to provide insights into the influence of drought on plantation trees in the study area.

Keywords: drought; NDVI; NDII; precipitation; El Niño; PDSI; forest disturbance; remote sensing; time series analysis

1. Introduction

Defined as an extended period of rainfall shortage coupled with higher than normal temperatures, droughts result in water shortages and plant water stress [1]. This prevalent, recurrent, and multifaceted feature of the climate system is widely recognized as one of the costliest natural catastrophes of the 20th century, threatening a multitude of terrestrial and aquatic ecosystems

worldwide [2] and holding serious implications for ecological and economic factors [3]. In forests, moisture and temperature anomalies associated with droughts affect the tree health, which often results in extensive tree mortality [4].

Past decades have witnessed a notable growth of drought studies reporting their varied impacts on forest ecosystems globally. Extended drought events have, in part, induced forest fires [5,6], provoked the outbreak and spread of tree-attacking insect pests [7], amplified tree moisture deficits [8], stimulated the establishment of opportunistic plant invaders [9,10], and engendered land degradation and fragmentation in and around forested landscapes [11]. These effects can result in severe tree mortality and incur heavy economic costs for the forestry industry [12,13]. This is a serious concern as [14] projected an increase in drought frequency, extent, and intensity, even in areas where droughts are irregular [13]. So, the effects of droughts cannot be ignored, because they present a compounding challenge to forest health and productivity [8,15,16].

Consistent and frequent monitoring of droughts across various scales is important for the forest industry in order to respond promptly to forest disturbances and so reduce the risk of damage [17]. This practice may enhance our understanding of the fundamental drivers that trigger droughts so that relevant forest management strategies can be developed [18], particularly in the face of shifting climate conditions [19]. Measurements based in situ have traditionally been used to monitor drought damage, although their spatial variability defies efforts to assess the ecological effects using field methods alone [20]. Moreover, drought monitoring requires high-density temporal data; satellite remote sensing provides necessary means to retrieve this information at flexible intervals, as well as to augment data derived in situ [21,22].

Progress in remote sensing, and, hence, the ability to detect droughts, has facilitated early warning systems [21] and the timely detection and monitoring of droughts across large areas [14]. The suite of the current generation of satellite imagers are capable of observing forest landscapes at much finer spatial scales than in the past and at a near-daily time step, enabling seamless reconstruction of the spatial and temporal manifestations of drought-mediated disturbances [23]. However, the understanding of droughts depends on the availability and consistency of satellite data. The opening of ample free satellite data archives by the United States (US) Geological Survey, coupled with the capacity to retrieve fully processed images [24,25] has transformed remote sensing into a practical means for monitoring droughts. Particularly, the Google Earth Engine (GEE) platform has become valuable for developing countries that are typically data-poor and lack high-performance computing systems for drought monitoring [26].

Typically, a remote sensing-based drought monitoring approach is achieved by tracking indices that reflect plant responses as an indicator of climate variability. Several vegetation indices exist, although the normalized difference vegetation index (NDVI) is the main, efficient, and commonly used one [27]. It is the measure of plant photosynthetic ability and productivity, which is a function of the difference between near-infrared (0.858 μm) and the red band (0.648 μm) reflectance over the combined reflectance in these two parts of the spectrum [20,28]. Vegetative drought conditions are described by a deviation of the NDVI values from their temporal mean, typically measured over extended time scales. Studies have established strong correlations between the NDVI values and the climatic variables [29], demonstrating that the index is an efficient indicator of climatic drought-driven vegetation changes [30]. Other important variables for the study of droughts are related to moisture storage in the root zone of the vegetation, which is measured by the normalized difference infrared index (NDII), and similar to the NDVI, it uses ratios of the near-infrared and short-wave infrared reflectance (1.65 μm) [31]. This is a robust indicator of water availability in the soil for use by trees [32].

To determine the influence of droughts on the vegetation, variations in the NDVI are often associated with drought indices, numerical criteria that characterize the drought intensity, scale, and duration by assimilating key environmental variables such as precipitation, temperature, and vegetation status [22]. The Palmer drought severity index (PDSI) is widely adopted [33], providing standardized moisture conditions over time by incorporating precipitation, temperature,

and potential evaporation [34]. The PDSI has been relatively successful at computing long-term drought conditions in several regions [33]. The index varies between −10 and +10 [35], where strong positive values represent extremely wet conditions, and strong negative ones indicate extreme drought. Here, we define a drought as a negative detrended NDVI as a response to a moisture deficit caused by climate variability.

In the eastern seaboard of South Africa, the 1991–1992 drought cost the forestry sector nearly R450 ($33.9) million [36]. During this period, more than 30,000 ha of forests were replanted shortly after the drought season, and a further expense of R2000 per hectare was incurred to replace the affected trees [37]. The most recent drought is closely comparable with that of 1991–1992 [38] and has been declared as the worst in 26 years [39,40]. Furthermore, [41], an agricultural industry association reported declining yields in other agricultural crops during 2016. However, in spite of their regular occurrence, the effects of droughts on forest plantations in this region have received little attention from scientists.

The effects of the recent drought on forest resources along the northeast coast of KwaZulu-Natal, South Africa have not been studied and are inconclusive. While previous drought effects on forests have been explored in South Africa, no past studies have employed remote sensing—this study is the first attempt to address this gap. Here, we use Moderate Resolution Imaging Spectroradiometer (MODIS)-derived NDVI and NDII coupled with climate variables over a 15-year period (2002−2016) to assess the influence of drought conditions on plantation forests in this region. MODIS was employed because of its informative characterization of drought events [42].

2. Materials and Methods

2.1. Study Area

The spatial context for this research is the KwaMbonambi plantation forests, which are located along the eastern seaboard of KwaZulu-Natal, 30 km northeast of Richards Bay (Figure 1). It is dominated by even-aged *Eucalyptus* L'Héritier. plantations of almost 40,000 ha. The plantations are managed by Sappi, a large South African pulp and paper company with a global reach. The growing stock mainly comprise 6–14-year-old *Eucalyptus grandis* W. Hill ex Maiden (*E. grandis*), *E. grandis* × *Eucalyptus camaldulensis* Dehnh. (*E. gxc*), and *E. grandis* × *Eucalyptus urophylla* S.T.Blake (*E. gxu*) hybrid clones. The stands are fairly uniform regarding canopy cover with tree density established at 1667 trees ha^{-1}. It is typical of the northern KwaZulu-Natal forestry region, which is subject to notable forest disturbances, such as fire and insect pest outbreaks. The area is characterized by a subtropical climate, and the mean annual temperature is 22 °C [43]. The area receives an annual rainfall averaging 1200 mm, which is highly seasonal and peaks between November and February [44], and the potential evapotranspiration is 1772 mm [45]. The landscape of KwaMbonambi is flat and consists of Quaternary alluvial sediments of clay sands of aeolian deposits [46] and soil with varying levels of organic matter [47], at an elevation of 74 m above sea level. The high penetrability of the soils permits prompt leaching of the nutrients due to the high rainfall in this region [46]. These conditions are favorable for fast-growing *Eucalyptus* plantations [48].

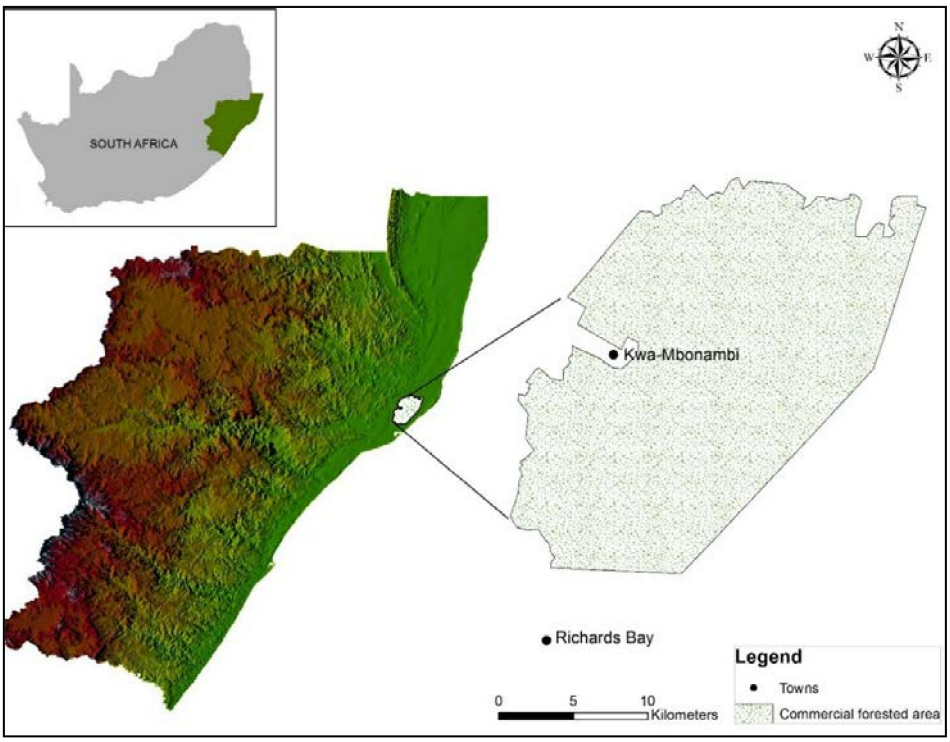

Figure 1. Location of KwaMbonambi along the northeast coast of KwaZulu-Natal, South Africa.

2.2. Data for NDVI and Climate Variables

Numerous Moderate Resolution Imaging Spectroradiometer (MODIS) products have been extensively used to monitor vegetation changes since 2000. In this study, we used the MODIS (MCD43A4) 16-day composite NDVI image product with 500-m resolution and nadir and bidirectional reflectance distribution function-adjusted spectral reflectance bands, because it reduces the anisotropic scattering effects of surfaces under different illumination and observation conditions [49]. The dataset provides a sample on a rolling 8-day interval based on 16 days of a MODIS surface reflectance composite period for bands 1–7. This product combines data from both the Terra and Aqua spacecrafts, taking the best representative pixel from the 16-day epoch [50]. The image collection ID: (MODIS/MCD43A4_NDVI) in the Google Earth Engine (GEE) environment was used to retrieve the MODIS data. The high temporal frequency of this product makes it possible to detect changes by using time series analysis, especially in the eastern seaboard of South Africa, where cloudy conditions present a challenge. Otherwise, a finer Landsat product is ideal for the unit scale of the study area, but data gaps were detected, and for that reason, the MODIS data was considered. The cloudy dates were filtered to obtain images captured under cloudless conditions and processed using the JavaScript code editor in the GEE environment. The NDVI values were averaged for the entire study area, and the mean annual NDVI was used for analysis. The NDII was calculated in the GEE environment using MODIS data.

To understand the NDVI–drought relationship, climatic factors that include PDSI, Niño 3.4, and precipitation were considered. Precipitation was also extracted from GEE using the Climate Engine Application (CEA, http://climateengine.org./). These data are generated from the Modern-Era Retrospective Analysis for Research Application (MERRA-2) model [51]. The MERRA model data are available at 0.67° × 0.50° resolution at 1–6 h intervals. The Niño 3.4 index is an index commonly used to quantify the strength and phase of the El Niño Southern Oscillation. El Niño events result from the anomalous warming of the eastern equatorial Pacific Ocean, which affects the circulation, often inducing drought and heat wave conditions over southern Africa via teleconnections [52,53]. The Niño 3.4 index was retrieved from the National Oceanic and Atmospheric Administration (NOAA)

online portal http://www.esrl.noaa.gov./psd/gcos_wgsp?Timeseries/. Niño 3.4 is computed by averaging sea–surface temperatures (SST) within the Niño 3.4 region, in this case 5° N–5° S latitude and 120° W–170° W latitude over the Pacific Ocean. The self-calibrating monthly Palmer drought severity index (PDSI) data were obtained from the University of East Anglia's Climatic Research Unit (CRU) (https://crudata.uea.ac.uk/cru/data/drought/). PDSI is computed from time series of precipitation and temperature, in conjunction with fixed parameters related to the soil/surface characteristics at each location [54].

2.3. Temporal Trend Analysis

The NDVI time series generally contains a strong seasonal component that is associated with the growing seasons of the vegetation [55]. The Breaks for Additive Seasonal and Trend (BFAST) method, an aligner tool, was applied to decompose the time series into the trend, seasonal, and random components, which explain seasonality and facilitate the detection of trend variations within the time series. The BFAST equation is given as follows:

$$y_t = m + T_t + S_t + R_t \tag{1}$$

where m is the mean, T is the trend component value, S is the seasonal component, and R is the random component at timestep t. The summation of the mean, trend, seasonal, and random components is equivalent to the original time series. Thereafter, the time series was "deseasonalized" using the "smoothTrend" function to remove the variations resulting from seasonal cycles.

Because the NDVI time series generally do not have normally distributed patterns and comprise non-linear trends and outliers [56], the Mann–Kendall test was applied to determine the significance of the 2002–2016 NDVI trend. A notable feature of this test is that it is insensitive to missing values and avoids the loss of seasonal information when inspecting the trend [57]. Following [58], the Mann–Kendall trend test is computed as follows:

$$S = \sum_{i=1}^{n-1} \sum_{j=i+1}^{n} \operatorname{sign}(T_j - T_i) \tag{2}$$

where

$$Sign(T_j - T_i) = \begin{cases} 1 \text{ if } T_j - T_i > 0 \\ 0 \text{ if } T_j - T_i = 0 \\ -1 \text{ if } T_j - T_i < 0 \end{cases} \tag{3}$$

where T_j and T_i are the annual values in years j and i, respectively, $j > i$. The average value of S is $E(S) = 0$, and the variance (σ^2) for the S statistic is given by the following:

$$\sigma^2 = \frac{n(n-1)(2n+5) - \sum t_i(i)(i-1)(2i+5)}{18} \tag{4}$$

in which t_i denotes the number of ties to extent i. The summation term in the numerator is used only if the data series contains tied values. The standard test statistic Z_s is calculated as follows:

$$Z_s = \begin{cases} \frac{s-1}{\sigma} for\ S > 0 \\ 0\ for\ S = 0 \\ \frac{s+1}{\sigma} for\ S < 0 \end{cases}. \tag{5}$$

The test statistic Z_s is used a measure of significance of the trend. In effect, this statistic is used in this study at a 95% confidence interval. If the z-score is between −1.96 and 1.96, then it implies that the trend is not significant, but if it falls outside this range, then the trend is significant.

2.4. Correlation Analysis of NDVI and Climate Factors

In this study, the Pearson correlation coefficient (r) between the NDVI, NDII, and climatic variables was calculated to assess the influence of climatic drought on the plantation trees. This method has been widely applied to analyze the relationship between the NDVI and climatic factors [59]. The strength of influence for climatic factors on the NDVI patterns was determined over the 15-year period, between 2002 and 2016.

3. Results

3.1. Drought Severity in Southern Africa

As an introduction to the general characteristics of the recent drought in terms of its strength and persistence, the El Niño events, which are associated with droughts in South Africa [60] are reconstructed in Figure 2. Severe droughts that affected the country were apparently established during a mature El Niño phase [61]. Over the past 30 years, the 1982–1983, 1991–1992, and 1994–1995 droughts appear to have been the most extreme, with the 1991–1992 drought declared as the worst on record [38]. However, this study, in agreement with [41] established that the recent drought is more severe and prolonged than the 1991–1992 event. In this regard, it was our intention to perform the analyses so that the effects of the recent drought on commercial forestry in South Africa are determined.

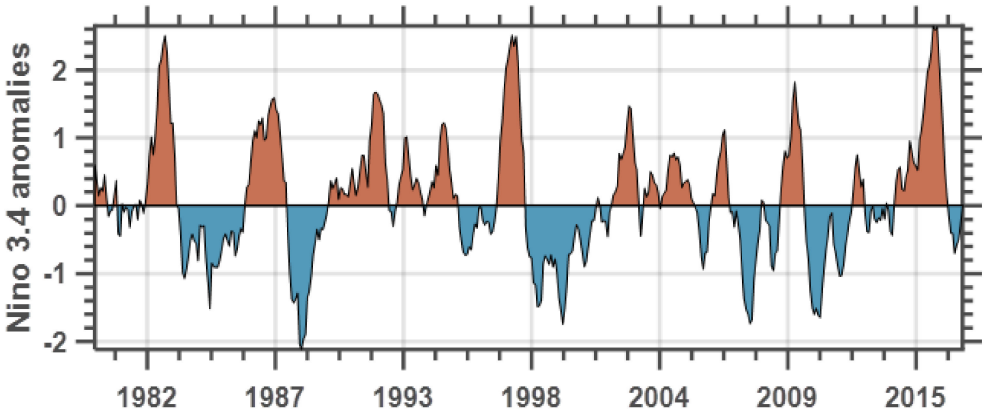

Figure 2. Standardized monthly Niño 3.4 anomalies from 1982 to 2016, showing warm (red) and cold (blue) phases of abnormal sea surface temperatures in the tropical Pacific Ocean.

3.2. Temporal Variability of NDVI

The temporal variability of the NDVI in the KwaMbonambi forest area is presented in Figure 3. The first panel shows the original NDVI time series, followed by the trend on which the analysis is based. The annual NDVI is fairly stable from 2002 until the breakpoint in 2014, which continues to decline until 2015. The plantation trees showed a relatively stable NDVI pattern between 2002 and 2013 (Figure 4), slightly decreased in 2014, and progressed further in 2015, with remnants of stable green over the eastern section. This difference suggests that the *Eucalyptus* clones in this region had varying sensitivity to drier conditions. While this may have been the case, there was no way to rule out the possible influence of other factors. In 2016, it seemed as if the plantations were recovering as evidenced by a slight increase in greening. This was confirmed by the smoothed NDVI time series (Figure 5), averaged for the entire study area with the shaded region showing the estimated 95% confidence intervals. The smaller brown (harvested) sites showed a patchy distribution, mostly in the eastern part of the study area, but appeared more prominently during the 2015 drought period. The permanent patch (timber site) southeast of the study area is an exception.

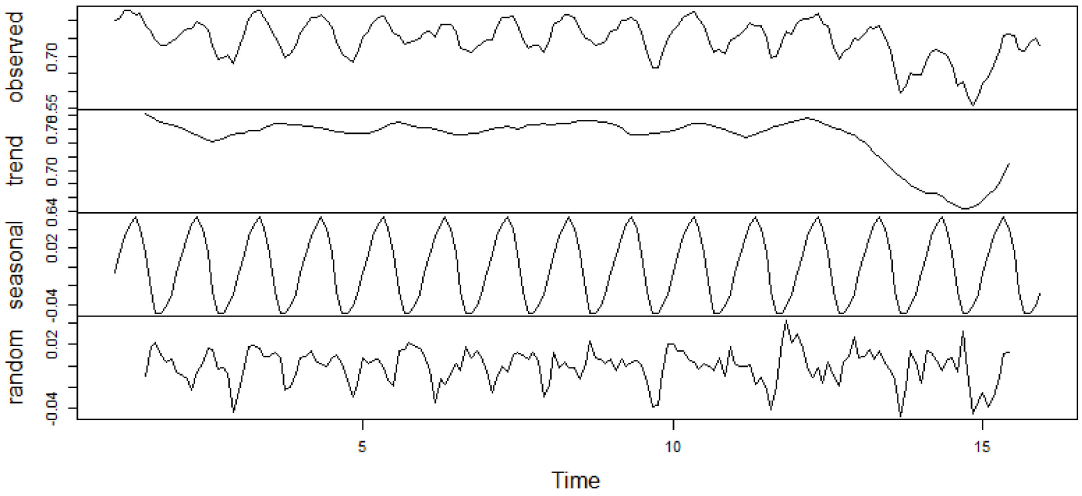

Figure 3. The Breaks for Additive Seasonal and Trend (BFAST) normalized difference vegetation index (NDVI) time series components of the entire area.

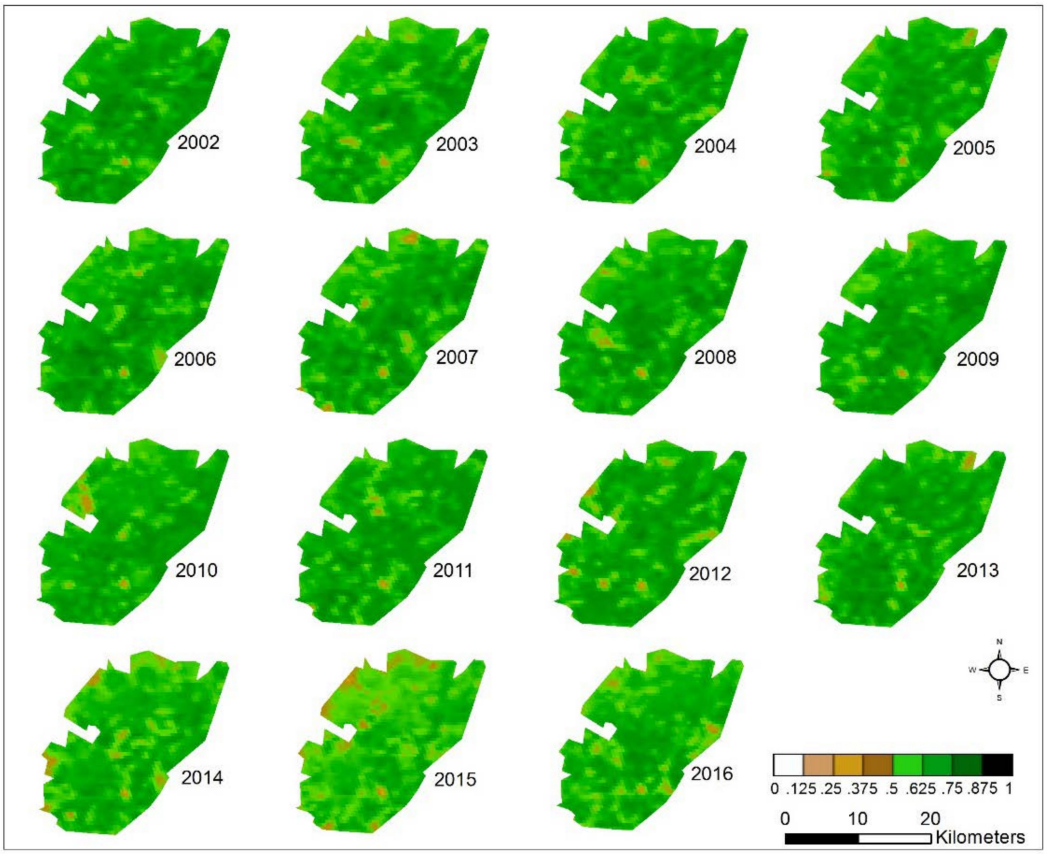

Figure 4. Temporal variability of NDVI from 2002 to 2016.

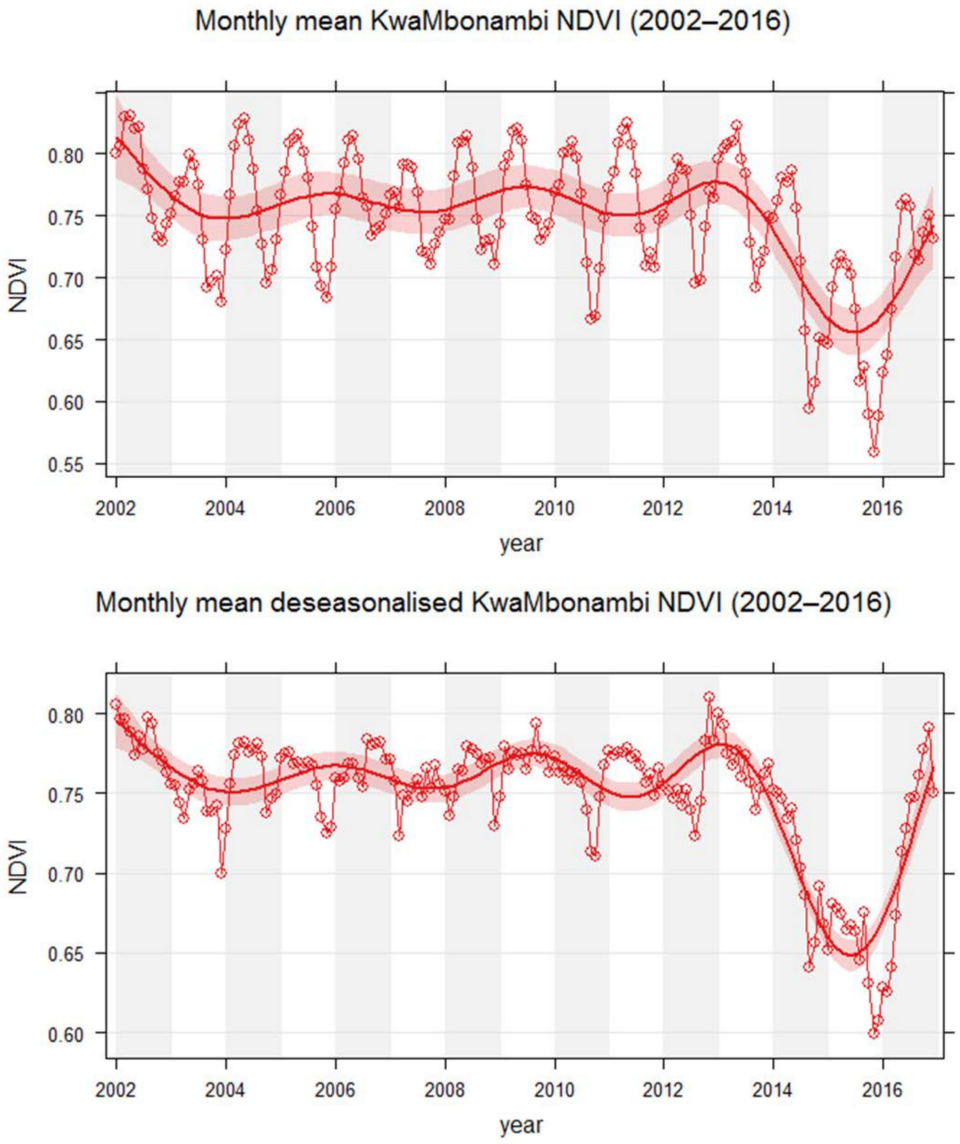

Figure 5. Smoothened and deseasonalised NDVI time series (2002–2016).

3.3. Time Series Analysis of NDVI, NDII, Precipitation, El Niño, and PDSI

The time series analysis of the NDVI and the climatic factors over the 15-year period from 2002 to 2016 is presented in Figure 6. The result shows a fairly constant NDVI pattern over the first 12 years, ranging between 0.74 and 0.78; it declined to 0.64 in 2015. This is supported by a Mann–Kendall test that showed a non-significant (p = 0.4661, z = −0.728) NDVI trend from 2002 to 2013. The trend (negative) was found to be significant from 2014 to 2015 (p = 0.000353, z = −3.5729). The NDVI was accompanied by a similar precipitation pattern (Figure 6b) with a shortage in 2015. The NDII (Figure 6d) also exhibited a similar pattern with the NDVI and precipitation. It can be seen from Figure 6d that the period of 2002–2013 had a high moisture content (NDII = 0.25), followed by a decrease in 2014 to drier conditions (NDII = 0.13) in 2015. From Figure 6a it is clear that the decrease in the NDVI is associated with the strongest (1.9) 2015 El Niño event, which led to 2015 being the hottest year on record globally [62]. The PDSI (−2.6) also pointed toward intense drought conditions during this period, as shown in Figure 6c. This was also confirmed by the lower NDII (0.13) value in 2015, which was indicative of a soil moisture deficit (Figure 6d). However, as shown in Figure 6a, the El Niño events after 2002 had little influence on the *Eucalyptus* trees compared with the recent event.

This was also supported by Figure 6c, which revealed that previous droughts over the study period surprisingly had a negligible effect on this valuable commodity. These results imply that the recent drought was relatively intense compared with other droughts events over the study period. Although not fully recovered in 2016, it seems that the NDVI is recovering, along with increasing precipitation while the El Niño effect is abating. So, the 2015–2016 drought appears to entail a temporal hiatus of the NDVI trend. However, given the cyclicity of droughts in this region, the apparent recovery trend remains to be confirmed.

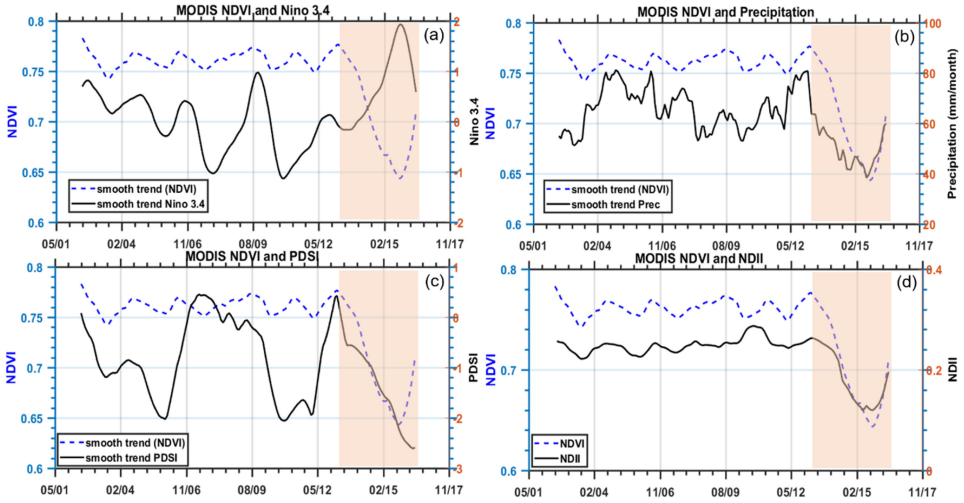

Figure 6. (**a**–**d**) Temporal variation of the NDVI, normalized difference infrared index (NDII), El Niño, Palmer drought severity index (PDSI), and precipitation from 2002 to 2016.

3.4. Correlation of NDVI, NDII, and Climatic Variation

The correlations of the NDVI, NDII, El Niño, PDSI, and precipitation are presented in Figure 7. The NDVI showed a strong correlation with the NDII ($r = 0.89$), highlighting the strength of the NDII to assess drought-related stress in the plantation trees. The results also indicated a negative correlation between El Niño and the NDVI ($r = -0.51$), as well as the NDII ($r = -0.53$), reaffirming the consistent mechanism of influence of drier conditions. The PDSI−NDVI correlation ($r = 0.34$) was also notable. Because the influence of the climate variables on the NDVI may not be stable throughout the study period, it was considered necessary to assess the extent to which the NDVI correlated with NDVII and the climate variables for each year (2002−2016).

The correlation coefficients presented in Figure 8 showed a strong NDVI–NDII relationship ($r > 0.7$) throughout the study period. The El Niño effect also showed a negative but strong correlation with the NDVI trends in 2015 ($r = -0.85$)—El Niños are well known to induce drier conditions in South Africa [63]. The relative NDVI decrement was strongly associated with the worsening PDSI signal, particularly in the period of 2013–2014 ($r = 0.9$) and 2015 ($r = 0.6$). On the other hand, the correlation of the NDVI and precipitation is not as high as the other variables ($r = 0.1$). In a similar study, [64] stressed that the correlation between the NDVI and precipitation is strongly influenced by the degree of aggregation over a time dimension. Moreover, studies such as [65] noted that the NDVI lags behind precipitation by several weeks or months. This is also the case in this study as illustrated in Figure 6b. Otherwise, the strong association of the NDII, PDSI, and El Niño with the NDVI confirms a decrease in the tree activity as a result of drier drought conditions in 2015. On the basis of these associations, therefore, it is apparent that the plantation trees during 2014–2015 suffered moisture stress because the El Niño was at its peak. This is reflected by a sharp decrease in greenness in 2015, as illustrated in Section 3.2.

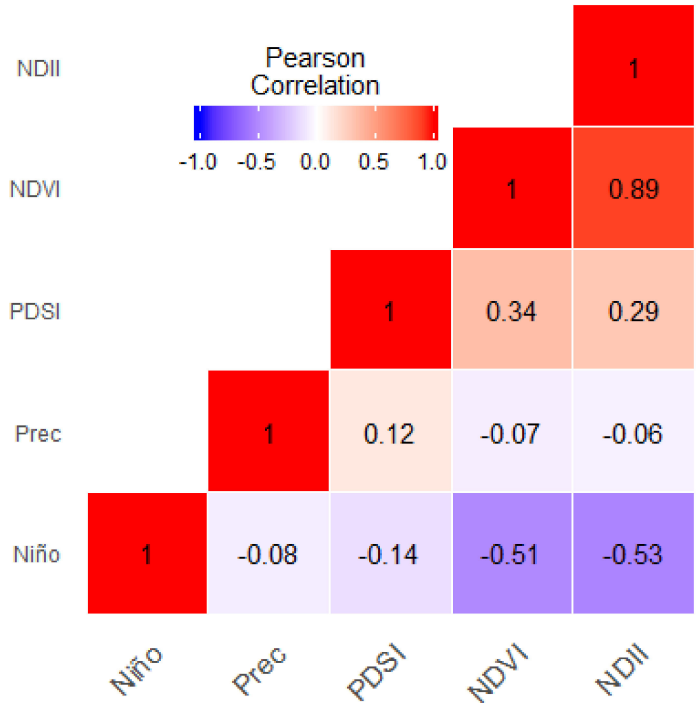

Figure 7. Pearson's correlation of the NDII, NDVI, PDSI, precipitation, and El Niño (2002–2016).

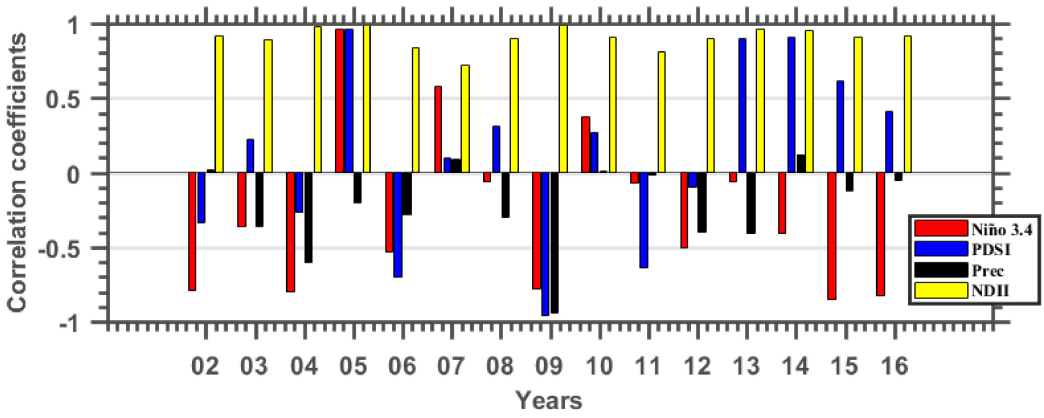

Figure 8. Pearson correlation coefficient of the NDVI, Niño, PDSI, precipitation and NDII for each year (2002–2016).

4. Discussion

We have explored the spatial variation and temporal patterns of the NDVI values as a surrogate for the plantation trees in association with climate variables. The plantations trees displayed high NDVI values in harmony with precipitation trends over much of the study period, until a sudden dip in 2014, which intensified further in 2015, reaffirming the consistent mechanism of influence [66,67], especially in arid and semi-arid regions where precipitation is the limiting factor for plant growth [68]. The NDII also exhibited a similar pattern with the NDVI and precipitation, suggesting that the reduction of tree activity in 2015 was related to a water deficit as a result of the strongest El Niño period, which is believed to have induced drier conditions [66] and altered vegetation reflectance spectra [69]. This reaffirms Sriwongsitanon's [31] finding that the NDII is a robust indicator of the interaction between precipitation, soil moisture, and plant water content. This further highlights the stronger influence of precipitation on tree activity [70]. In accordance with this observation,

the negative PDSI signal pointed towards a severe drought event that had already been reported by [38,41] as the worst over the past four decades in this country. This drought was notable because of its severity and duration. In response, the plantation trees exhibited a sharp drop of greenness as the NDVI reached a value of 0.64—the lowest recorded over the study period, with the exception of clones over the central east region that showed tolerance. More recently, in KwaMbonambi, [71] found large-scale dieback of a single *E. gxu* hybrid clone, while other *E. gxu* clones in the same area remained relatively healthy. Following this finding, intensive assessments were carried out to consider the possible role of insect pests and pathogens on the affected trees, and the results showed no evidence that these disturbances were responsible for the dieback [71]. Instead, their results showed variation in the hydraulic functioning among the *E. gxu* clones, where dying clones suffered from drier field conditions compared with other healthier clones.

This is also supported by the extended reduced precipitation over the same period. For this purpose, [61] advised that the advent of El Niño conditions should signify to key stakeholders the probability of severe drought effects. To maintain maximum productivity in the face of threatening climate variability, scientists have long been adjusting and developing crop hybrids that can survive drier conditions [72]. Nevertheless, the El Niño-mediated droughts are most frequent in South Africa [38] and hold important implications not only for the forestry sector but also water resources, food systems, and the socio-economic welfare of the country. Otherwise, the performance of the NDVI and the NDII in detecting the 2015 drought was comparable, with the NDVI showing slightly more sensitivity. In other related studies [32], the NDII was found to react to drought conditions faster and to greater extent than the NDVI. Furthermore, the analyses between the NDVI, NDII, and climate variables using the BFAST time series method proved to be a robust tool for probing forest ecosystem function responses to climate variability [73,74].

The overall impression is that these findings for 2015 indicate several landscape scenarios with implications for forest productivity in northeastern South Africa. First, that the plantation trees appeared to have suffered from moisture stress, as evidenced by the decrease in the NDVI and the NDII; second, that a clear variation in the NDVI was apparent, suggesting that some clones were more sensitive to climate variation than others. This is consistent with [75] who established that the variation in canopy response to water availability has been recorded for many *Eucalyptus* clones in South Africa; and lastly, based on these conditions, the growth of drought-sensitive clones was affected.

The method demonstrated in this study can be applied on a broader scale and to other drought-prone areas to help provide greater economic security of the plantation forests. Particularly, the GEE platform enables the efficient characterization of the plantations' responses to droughts with minimal data processing [26]. This holds much promise to address Huang's [71] concerns that drought monitoring at regional to global scales are challenging.

5. Conclusions

This study provides the first demonstration of the influence of drought on the plantation forest tree activity in South Africa using high-density satellite time series data. The analyses of the NDVI, NDII, and climatic variables offered a more detailed account of the spatiotemporal effects of drought conditions on *Eucalyptus* plantations. The results showed a positive correlation of the NDVI with the NDII and precipitation; all declined sharply in 2015. This decrease was associated with a strong El Niño event, which is credited with inducing drier conditions over this period. Severe drought was apparent in 2015, as confirmed by a negative (−2.6) PDSI and a low (0.13) NDII value, suggesting a soil moisture deficit. In light of these results, we concluded that the vegetation activity of the *Eucalyptus* species in KwaMbonambi responded with varying sensitivity to the 2015 drought event. For that reason, we support the suggestion by [76] that drought-tolerant clones can be an ideal substitute for sensitive ones. In addition, it would be desirable to evaluate how different clones react to climatic variability and to evaluate these variables on a larger scale. Lastly, the MODIS-derived NDVI and

NDII proved to be reliable indicators for the temporal pattern of drought conditions and provided an efficient means for characterizing plantations and their response to climate variability.

Overall, the results highlight the great potential of the GEE platform in refining our ability to map forest responses to climate variability. Through free access to ready-to-use satellite data, along with continuous algorithm developments, the retrieval of temporal drought effects on plantation forests is now possible. This offers a promising outlook for uncovering key disturbance patterns, which will enable a much-improved understanding of complex forest processes in the face of the changing climate.

Author Contributions: Conceptualization, S.X., M.G., K.P., and R.I.; Methodology, Formal Analysis, Resources, Writing of Original Draft, S.X.; and Review and Editing of Final Manuscript: S.X., M.G., K.P., and R.I.

Funding: This research was partly funded by the South African National Space Agency (SANSA).

Acknowledgments: We would like to thank Nkanyiso Mbatha for his assistance with the data gathering and presentation. The authors would also like to thank Graham Baker for editing this paper. Lastly, the three anonymous reviewers are thanked for providing constructive comments, which greatly improved the manuscript.

Conflicts of Interest: The authors declare no conflicts of interest.

References

1. Solh, M.; van Ginkel, M. Drought preparedness and drought mitigation in the developing world's drylands. *Weather Clim. Extremes* **2014**, *3*, 62–66. [CrossRef]
2. Bayissa, Y.; Tadesse, T.; Demisse, G.; Shiferaw, A. Evaluation of satellite-based rainfall estimates and application to monitor meteorological drought for the Upper Blue Nile Basin, Ethiopia. *Remote Sens.* **2017**, *9*, 669. [CrossRef]
3. Mokhtari, A.; Mansor, S.B.; Mahmud, A.R.; Helmi, Z.M. Monitoring the impacts of drought on land use/cover: A developed object-based algorithm for NOAA AVHRR time series data. *J. Appl. Sci.* **2011**, *11*, 3089–3103. [CrossRef]
4. Millar, C.I.; Stephenson, N.L. Temperate forest health in an era of emerging megadisturbance. *Science* **2015**, *349*, 823–826. [CrossRef] [PubMed]
5. Alencar, A.A.; Solórzano, L.A.; Nepstad, D.C. Modeling forest understory fires in an eastern Amazonian landscape. *Ecol. Appl.* **2004**, *14*, 139–149. [CrossRef]
6. Pausas, J.G. Changes in fire and climate in the eastern Iberian Peninsula (Mediterranean Basin). *Clim. Chang.* **2004**, *63*, 337–350. [CrossRef]
7. Kolb, T.E.; Fetting, C.J.; Ayres, M.P.; Bentz, B.J.; Hicke, J.A.; Mathiasen, R.; Stewart, J.E.; Weed, A.S. Observed and anticipated impacts of drought on forest insects and diseases in the United States. *For. Ecol. Manag.* **2016**, *380*, 321–334. [CrossRef]
8. Asner, G.P.; Brodrick, P.G.; Anderson, C.B.; Vaughn, N.; Knapp, D.E.; Martin, R.E. Progressive forest canopy water loss during the 2012–2015 California drought. *Proc. Natl. Acad. Sci. USA* **2016**, *113*, E249–E255. [CrossRef] [PubMed]
9. Weed, A.S.; Ayres, M.P.; Hicke, J.A. Consequences of climate change for biotic disturbances in North American forests. *Ecol. Monogr.* **2013**, *83*, 441–470. [CrossRef]
10. Laube, J.; Ziegler, K.; Sparks, T.H.; Estrella, N.; Menzel, A. Tolerance of alien plant species to extreme events is comparable to that of their native relatives. *Preslia* **2015**, *87*, 31–53.
11. Bruins, H.J.; Berliner, P.R. *Bioclimatic Aridity, Climatic Variability, Drought and Desertification: Definitions and Management Options*; Springer: Dordrecht, The Netherlands, 1998.
12. McIntyre, P.J.; Thorne, J.H.; Dolanc, C.R.; Flint, A.L.; Flint, L.E.; Kelly, M.; Ackerly, D.D. Twentieth-century shifts in forest structure in California: Denser forests, smaller trees, and increased dominance of oaks. *Proc. Natl. Acad. Sci. USA* **2015**, *112*, 1458–1463. [CrossRef] [PubMed]
13. Clark, J.S.; Iverson, L.; Woodall, C.W.; Allen, C.D.; Bell, D.M.; Bragg, D.C.; Jackson, S.T. The impacts of increasing drought on forest dynamics, structure, and biodiversity in the United States. *Glob. Chang. Biol.* **2016**, *22*, 2329–2352. [CrossRef] [PubMed]
14. Norman, S.P.; Koch, F.H.; Hargrove, W.W. Review of broad-scale drought monitoring of forests: Toward an integrated data mining approach. *For. Ecol. Manag.* **2016**, *380*, 346–358. [CrossRef]

15. Allen, C.D.; Breshears, D.D.; McDowell, N.G. On underestimation of global vulnerability to tree mortality and forest die-off from hotter drought in the Anthropocene. *Ecosphere* **2015**, *6*, 1–55. [CrossRef]
16. Young, D.J.N.; Stevens, J.T.; Earles, J.M.; Moore, J.; Ellis, A.; Jirka, A.L.; Latimer, A.M. Long-term climate and competition explain forest mortality patterns under extreme drought. *Ecol. Lett.* **2017**, *20*, 78–86. [CrossRef] [PubMed]
17. Byer, S.; Jin, Y. Detecting drought-induced tree mortality in sierra nevada forests with time series of satellite data. *Remote Sens.* **2017**, *9*, 929. [CrossRef]
18. Martínez-Vilalta, J.; Lloret, F.; Breshears, D.D. Drought-induced forest decline: Causes, scope and implications. *Biol. Lett.* **2012**, *8*, 689–691. [CrossRef] [PubMed]
19. Neumann, M.; Mues, V.; Moreno, A.; Hasenauer, H.; Seidl, R. Climate variability drives recent tree mortality in Europe. *Glob. Chang. Biol.* **2017**, *23*, 4788–4797. [CrossRef] [PubMed]
20. Asner, G.P.; Alencar, A. Drought impacts on the Amazon forest: The remote sensing perspective. *New Phytol.* **2010**, *187*, 569–578. [CrossRef] [PubMed]
21. Hayes, M.J.; Svoboda, M.D.; Wardlow, B.D.; Anderson, M.C.; Kogan, F. *Drought Monitoring: Historical and Current Perspectives*; CRC Press: Boca Raton, FL, USA, 2012.
22. Rao, M.; Silber-Coats, Z.; Powers, S.; Fox, L.; Ghulam, A. Mapping drought-impacted vegetation stress in California using remote sensing. *GISci. Remote Sens.* **2017**, *54*, 185–201. [CrossRef]
23. Park, S.; Im, J.; Park, S.; Rhee, J. Drought monitoring using high resolution soil moisture through multi-sensor satellite data fusion over the Korean peninsula. *Agric. For. Meteorol.* **2017**, *237*, 257–269. [CrossRef]
24. Roy, D.P.; Wulder, M.A.; Loveland, T.R.; Woodcock, C.E.; Allen, R.G.; Anderson, M.C.; Scambos, T.A. Landsat-8: Science and product vision for terrestrial global change research. *Remote Sens. Environ.* **2014**, *145*, 154–172. [CrossRef]
25. Wulder, M.A.; White, J.C.; Loveland, T.R.; Woodcock, C.E.; Belward, A.S.; Cohen, W.B.; Roy, D.P. The global Landsat archive: Status, consolidation, and direction. *Remote Sens. Environ.* **2016**, *185*, 271–283. [CrossRef]
26. Sazib, N.; Mladenova, I.; Bolten, J. Leveraging the Google Earth Engine for drought assessment using Global Soil Moisture Data. *Remote Sens.* **2018**, *10*, 1265. [CrossRef]
27. Liu, H.Q.; Huete, A.A. A feedback based modification of the NDVI to minimize canopy background and atmospheric noise. *IEEE Trans. Geosci. Remote Sens.* **1995**, *33*, 457–465.
28. Guo, X.Y.; Zhang, H.Y.; Wang, Y.Q.; He, H.S.; Wu, Z.F.; Jin, Y.H.; Zhao, J.J. Comparison of the spatio-temporal dynamics of vegetation between the Changbai Mountains of eastern Eurasia and the Appalachian Mountains of eastern North America. *J. Mt. Sci.* **2018**, *15*, 1–12. [CrossRef]
29. Piao, S.; Mohammat, A.; Fang, J.; Cai, Q.; Feng, J. NDVI-based increase in growth of temperate grasslands and its responses to climate changes in China. *Glob. Environ. Chang.* **2006**, *16*, 340–348. [CrossRef]
30. Wardlow, B.D.; Anderson, M.C.; Verdin, J.P. *Remote Sensing of Drought: Innovative Monitoring Approaches*; CRC Press: Boca Raton, FL, USA, 2012.
31. Sriwongsitanon, N.; Gao, H.; Savenije, H.H.G.; Maekan, E.; Saengsawan, S.; Thianpopirug, S. The Normalized Difference Infrared Index (NDII) as a proxy for soil moisture storage in hydrological modelling. *Hydrol. Earth Syst. Sci. Discuss.* **2015**, *12*, 8419–8457. [CrossRef]
32. Sriwongsitanon, N.; Gao, H.; Savenije, H.H.G.; Maekan, E.; Saengsawan, S.; Thianpopirug, S. Comparing the Normalized Difference Infrared Index (NDII) with root zone storage in a lumped conceptual model. *Hydrol. Earth Syst. Sci.* **2016**, *20*, 3361–3377. [CrossRef]
33. Beyaztas, U.; Arikan, B.B.; Beyaztas, B.H.; Kahya, E. Construction of prediction intervals for Palmer drought severity index using bootstrap. *J. Hydrol.* **2018**, *559*, 461–470. [CrossRef]
34. Mika, J.; Horvath, S.Z.; Makra, L.; Dunkel, Z. The Palmer Drought Severity Index (PDSI) as an indicator of soil moisture. *Phys. Chem. Earth Parts A/B/C* **2005**, *30*, 223–230. [CrossRef]
35. Hayes, M.; Svoboda, M.D.; Wall, N.; Widhalm, M. The Lincoln declaration on drought indices: Universal meteorological drought index recommended. *Bull. Am. Meteorol. Soc.* **2011**, *92*, 485–488. [CrossRef]
36. Warburton, M.; Schulze, R. *Climate Change and the South African Commercial Forestry Sector: An Initial Study*; ACRUcons Report 54; Report to Forestry SA: Pietermaritzburg, South Africa, 2006.
37. Dube, L.T.; Jury, M.R. The nature of climate variability and impacts of drought over KwaZulu-Natal, South Africa. *S. Afr. Geogr. J.* **2000**, *82*, 44–53. [CrossRef]
38. Baudoin, M.A.; Vogel, C.; Nortje, K.; Naik, M. Living with drought in South Africa: Lessons learnt from the recent El Niño drought period. *Int. J. Disaster Risk Reduct.* **2017**, *23*, 128–137. [CrossRef]

39. DAFF (Department of Agriculture, Forestry and Fisheries). *Drought Relief Update and the Country's Readiness to Import Grains*; Department of Agriculture, Forestry and Fisheries: Pretoria, South Africa, 2016.
40. Vogel, C.; van Zyl, K. Drought: In search of sustainable solutions to a persistent, 'wicked' problem in South Africa. In *Climate Change Adaptation Strategies—An Upstream-Downstream Perspective*; Springer: Cham, Switzerland, 2016.
41. AgriSA. *A Rain Drop in the Drought. Report to the Mulfi-Stakeholder Task Team on the Drought—Agri SA's Status Report on the Current Drought Crisis, Viewed*; Agri South Africa: Pretoria, South Africa, 2016.
42. Assal, T.J.; Anderson, P.J.; Sibold, J. Spatial and temporal trends of drought effects in a heterogeneous semi-arid forest ecosystem. *For. Ecol. Manag.* **2016**, *365*, 137–151. [CrossRef]
43. Department of Water Affairs and Forestry (DWAF). *Water Resource Protection and Assessment Policy Implementation Process. Resource Directed Measures for Protection of Water Resource: Methodology for the Determination of the Ecological Water Requirements for Estuaries*; Department of Water Affairs and Forestry: Pretoria, South Africa, 2004.
44. Dovey, S.B. Effects of Clear Felling and Residue Management on Nutrient Pools, Productivity and Sustainability in a Clonal *Eucalypt* Stand in South Africa. Ph.D. Thesis, Stellenbosch University, Stellenbosch, South Africa, 2012.
45. Little, K.; Rolando, C. The impact of vegetation control on the establishment of pine at four sites in the summer rainfall region of South Africa. *S. Afr. For. J.* **2001**, *192*, 31–39. [CrossRef]
46. Mucina, L.; Rutherford, M.C. *The Vegetation of South Africa, Lesotho and Swaziland*; South African National Biodiversity Institute: Pretoria, South Africa, 2006.
47. Luvuno, L.; Kotze, D.; Kirkman, K. Long-term landscape changes in vegetation structure: Fire management in the wetlands of KwaMbonambi, South Africa. *Afr. J. Aquat. Sci.* **2016**, *41*, 279–288. [CrossRef]
48. Lesch, W.; Scott, D.F. The response in water yield to the thinning of *Pinus radiata*, *Pinus patula* and *Eucalyptus grandis* plantations. *For. Ecol. Manag.* **1997**, *99*, 295–307. [CrossRef]
49. Schaaf, C.B.; Gao, F.; Strahler, A.H.; Lucht, W.; Li, X.; Tsang, T.; Strugnell, N.C.; Zhang, X.; Jin, Y.; Muller, J.P.; et al. First operational BRDF, albedo nadir reflectance products from MODIS. *Remote Sens. Environ.* **2002**, *83*, 135–148. [CrossRef]
50. Salmon, B.P.; Olivier, J.C.; Kleynhans, W.; Wessels, K.J.; van den Bergh, F.; Steenkamp, K.C. The use of a multilayer perceptron for detecting new human settlements from a time series of MODIS images. *Int. J. Appl. Earth Obs. Geoinform.* **2011**, *13*, 873–883. [CrossRef]
51. Reinecker, M.M.; Suarez, M.J.; Gelaro, R.; Todling, R.; Bacmeister, J.; Liu, E.; Bosilovich, M.G.; Schubert, S.D.; Takacs, L.; Kim, G.K.; et al. MERRA: NASA's modern-era retrospective analysis for research and applications. *J. Clim.* **2011**, *24*, 3624–3648. [CrossRef]
52. Halpert, M.S.; Ropelewski, C.F. Surface temperature patterns associated with the Southern Oscillation. *J. Clim.* **1992**, *5*, 577–593. [CrossRef]
53. Ropelewski, C.F.; Halpert, M.S. Global and regional scale precipitation patterns associated with the El Niño/Southern Oscillation. *Mon. Weather Rev.* **1987**, *115*, 1606–1626. [CrossRef]
54. Van der Schrier, G.; Barichivich, J.; Briffa, K.R.; Jones, P.D. A scPDSI-based global data set of dry and wet spells for 1901–2009. *J. Geophys. Res. Atmos.* **2013**, *118*, 4025–4048. [CrossRef]
55. Jong, R.; Verbesselt, J.; Schaepman, M.E.; de Bruin, S. Trend changes in global greening and browning: Contribution of short-term trends to longer-term change. *Glob. Chang. Biol.* **2012**, *18*, 642–655. [CrossRef]
56. Birsan, M.V.; Molnar, P.; Burlando, P.; Pfaundler, M. Streamflow trends in Switzerland. *J. Hydrol.* **2005**, *314*, 312–329. [CrossRef]
57. Alcaraz-Segura, D.; Liras, E.; Tabik, S.; Paruelo, J.; Cabello, J. Evaluating the consistency of the 1982–1999 NDVI trends in the Iberian Peninsula across four time-series derived from the AVHRR sensor: LTDR, GIMMS, FASIR, and PAL-II. *Sensors* **2010**, *10*, 1291–1314. [CrossRef] [PubMed]
58. Pohlert, T. Non-Parametric Trend Tests and Change-Point Detection. 2018. Available online: https://cran.r-project.org/web/packages/trend/trend.pdf (accessed on 12 April 2018).
59. Jiang, L.L.; Jiapaer, G.; Bao, A.M.; Guo, H.; Ndayisaba, F. Vegetation dynamics and responses to climate change and human activities in central Asia. *Sci. Total Environ.* **2017**, *599*, 967–980. [CrossRef] [PubMed]
60. Fauchereau, N.; Trzaska, S.; Rouault, M.; Richard, Y. Rainfall variability and changes in southern Africa during the 20th century in the global warming context. *Nat. Hazards* **2003**, *29*, 139–154. [CrossRef]

61. Rouault, M.; Richard, Y. Intensity and spatial extension of drought in South Africa at different time scales. *Water SA* **2003**, *29*, 489–500. [CrossRef]
62. Tollefson, J. 2015 breaks heat record: Pacific Ocean warming helped to make last year the hottest in history. *Nature* **2016**, *529*, 450–451. [PubMed]
63. Richard, Y.; Trzaska, S.; Roucou, P.; Rouault, M. Modification of the southern African rainfall variability/ENSO relationship since the late 1960s. *Clim. Dyn.* **2000**, *16*, 883–895. [CrossRef]
64. Wang, J.; Rich, P.M.; Price, K.P. Temporal responses of NDVI to precipitation and temperature in the central Great Plains, USA. *Int. J. Remote Sens.* **2003**, *24*, 2345–2364. [CrossRef]
65. Udelhoven, T.; Stellmes, M.; del Barrio, G.; Hill, J. Assessment of rainfall and NDVI anomalies in Spain (1989–1999) using distributed lag models. *Int. J. Remote Sens.* **2009**, *30*, 1961–1976. [CrossRef]
66. Liu, G.; Liu, H.; Yin, Y. Global patterns of NDVI-indicated vegetation extremes and their sensitivity to climate extremes. *Environ. Res. Lett.* **2013**, *8*. [CrossRef]
67. Bachmair, S.; Tanguy, M.; Hannaford, J. How well do meteorological indicators represent agricultural and forest drought across Europe? *Environ. Res. Lett.* **2018**, *13*, 34–42. [CrossRef]
68. Song, Y.; Ma, M. A statistical analysis of the relationship between climatic factors and the Normalized Difference Vegetation Index in China. *Int. J. Remote Sens.* **2011**, *32*, 3947–3965. [CrossRef]
69. Huemmrich, K.F.; Kinoshita, G.; Gamon, J.A.; Houston, S.; Kwon, H.; Oechel, W.C. Tundra carbon balance under varying temperature and moisture regimes. *J. Geophys. Res. Biogeosci.* **2010**, *115*. [CrossRef]
70. Formica, A.F.; Burnside, R.J.; Dolman, P.M. Rainfall validates MODIS-derived NDVI as an index of spatio-temporal variation in green biomass across non-montane semi-arid and arid Central Asia. *J. Arid Environ.* **2017**, *142*, 11–21. [CrossRef]
71. Crous, C.J.; Greyling, I.; Wingfield, M.J. Dissimilar stem and leaf hydrailic traits suggest varying drought tolerance among co-occurring *Eucalyptus grandis* × *E.urophylla* clones. *South. For. J. For. Sci.* **2018**, *80*, 175–184. [CrossRef]
72. Forestry South Africa. Climate Change: A Forest for Forestry. 2016. Available online: http://www.forestry.co.za/climate-change-a-forecast-for-forestry/ (accessed on 10 April 2018).
73. Huang, K.; Zhou, T.; Zhao, X. Extreme drought-induced trend changes in MODIS EVI time series in Yunnan, China. *IOP Conf. Ser. Earth Environ. Sci.* **2014**, *17*, 012070. [CrossRef]
74. Piao, S.; Fang, J.; Zhou, L.; Ciais, P.; Zhu, B. Variations in satellite-derived phenology in China's temperate vegetation. *Glob. Chang. Biol.* **2006**, *12*, 672–685. [CrossRef]
75. Eksteen, A.B.; Grzeskowiak, V.; Jones, N.B.; Pammenter, N.W. Stomatal characteristics of *Eucalyptus grandis* clonal hybrids in response to water stress. *South. For. J. For. Sci.* **2013**, *75*, 105–111. [CrossRef]
76. Herrero, A.; Zamora, R. Plant responses to extreme climatic events: A field test of resilience capacity at the southern range edge. *PLoS ONE* **2014**, *9*. [CrossRef] [PubMed]

© 2018 by the authors. Licensee MDPI, Basel, Switzerland. This article is an open access article distributed under the terms and conditions of the Creative Commons Attribution (CC BY) license (http://creativecommons.org/licenses/by/4.0/).